Article | Received 7 March 2024; Accepted 7 September 2024; Published 14 September 2024
https://doi.org/10.55092/am20240013

Friction properties of SLM formed Ti48Al2Cr2Nb alloy

Zhanyong Zhao[1,]*, Yongli Guo[1], Wenbo Du[2], Peikang Bai[1,3,]*, Zhen Zhang[1], Liqing Wang[1], Kai Ma[1] and Yaohao Du[1]

1 School of Materials Science and Engineering, North University of China, Taiyuan 030051, China

2 National Key Laboratory for Remanufacturing, Academy of Army Armored Forces, Beijing 100072, China

3 College of Materials Science and Engineering, Taiyuan University of Science and Technology, Taiyuan 030024, China

* Correspondence authors; E-mails: zhaozy@nuc.edu.cn (Z. Z.); baipeikang@nuc.edu.cn (P. B.).

Abstract: Ti48Al2Cr2Nb alloy was prepared by selective laser melting (SLM). The effects of different rotational speeds on the friction properties of Ti48Al2Cr2Nb alloy and the alloy after hot isostatic pressing (HIP) were studied. The results are as follows: (1) With the increase of rotational speeds, the wear rate of Ti48Al2Cr2Nb alloy decreases and the friction coefficient decreases gradually. This is due to the formation of a mechanical mixed layer, which reduces the contact area between the friction material and the wear surface and improves the tribological properties. (2) After HIP treatment, the wear rate is greatly reduced, and some large flake wear debris appear on the wear surface. This is because the hardness of the material after HIP treatment becomes larger, and it has strong wear resistance and cutting resistance. However, the crystal structure inside is dense and orderly, and it is difficult to deform plastically, which is prone to brittle fracture. (3) When the rotational speeds is 400 r/min, the friction coefficient is the lowest. The reason is that the sample has low hardness and good plasticity. At high speeds, the material will deform, plastic flow and disperse mixing, forming a large number of thick mechanical mixing layers.

Keywords: selective laser melting; Ti48Al2Cr2Nb alloy; microstructure; tribological behavior; wear-resistant

1. Introduction

With the smooth and orderly development of the manned lunar landing project, the engine of the new spacecraft has higher requirements, requiring higher temperature, lighter weight and higher efficiency. Therefore, it is necessary to have more advanced design concepts, in which improving the performance of high-temperature materials is the key to improving the engine of the aircraft. At present, the high temperature alloys widely used in aerospace are Ni-based and Ti-based alloys. However, the current research on their high temperature properties is close to the limit, and their density is large, which cannot meet the requirements of new engine lightweight. The development of new high temperature materials has become the key to the development of national aerospace field [1–4].

Intermetallic compounds have high heat resistance, high specific strength, high specific life, high thermal conductivity and high oxidation resistance, as well as toughness and good thermal processing properties superior to ceramic materials, which are considered to be ideal high temperature resistant materials, and have received extensive attention from various countries [5,6]. TiAl alloy has high melting point, low density, high specific strength, high high temperature strength and creep resistance, and its service temperature can reach more than 1000 °C [7,8]. Compared with traditional Ni-based and Ti-based alloys, it can be seen from Table 1 [9] that γ-TiAl is more suitable for high temperature alloys except for poor plasticity. This kind of alloy usually contains a small amount of α_2-T_3Al phase. Compared with Ni-based alloy, the density of TiAl alloy is only about half of that of Ni-based alloy, and the elastic modulus, tensile strength and creep resistance limit of TiAl alloy are slightly lower than those of Ni-based alloy. Compared with Ti-based alloy, the density of TiAl alloy is slightly smaller, and the elastic modulus, creep resistance limit and oxidation resistance limit are slightly higher than those of Ti alloy [10].

Table 1. Properties of titanium aluminide, titanium alloy and nickel based super alloy.

Property	Ti-base alloy	TiAl-base alloy	Ni-base alloy
Density/(g/cm^3)	4.5	3.7–3.9	7.9–8.5
Elastic modulus/GPa	95–115	160–176	206
Yield strength/MPa	380–1150	400–630	800–1200
Tensile strength/MPa	480–1200	450–700	1250–1450
Creep limit/°C	600	1000	800–1090
$\delta_{5,\ RT}$/%	10–25	1–3	3–25

The alloying elements of TiAl alloys are one of the important factors affecting their properties and applications [11,12]. Ni is a common alloying element, which can significantly improve the mechanical properties and high temperature stability of TiAl alloys [13,14]. Adding a certain amount of niobium can improve the yield strength, plasticity and high temperature oxidation resistance of TiAl alloy. YOSHIHARA *et al.* [15] studied the oxidation behavior of γ-TiAl alloys, and found that the addition of Nb inhibited the growth of oxide TiO_2 and reduced the difference of thermal expansion coefficient between the alloy and the oxide. Cr can improve the oxidation resistance and high temperature hardness of TiAl alloy, but has little effect on its strength and plasticity. The second generation TiAl alloy

(Ti48Al2Cr2Nb) first developed by BARTOLOTTA P *et al.* [16] has good mechanical properties. The addition of Cr element improves the room temperature plasticity of TiAl alloy [17]. Ti and Al are the main alloying elements of TiAl alloys, but too high titanium content will lead to increased brittleness of the alloy. In general, the content of titanium in TiAl alloys for engineering should be controlled between about 42–48%. IMAYEV *et al.* [18] studied the effect of aluminum content and further addition of other alloying elements on the microstructure of TiAl alloy. The results show that some alloy components can obtain fine and uniform microstructure without strong segregation by β phase solidification.

Ti48Al2Cr2Nb alloy is an intermetallic compound based on titanium and aluminum. It has excellent properties such as low density, high specific strength and high temperature strength. It is considered to be a new structural material with wide application prospects. Selective laser melting of TiAl alloy can make up for the difficulty of forming complex structural parts by traditional forming methods. However, the research on the friction properties of SLM formed Ti48Al2Cr2Nb alloy is still limited, and further research is needed to explore the friction properties of the alloy and its influencing factors.

In this paper, the friction and wear properties of SLM formed Ti48Al2Cr2Nb alloy before and after hot isostatic pressing were studied. The wear surface, cross section and wear debris of SLM formed Ti48Al2Cr2Nb alloy at different rotational speeds were analyzed, and the wear mechanism of SLM formed Ti48Al2Cr2Nb alloy before and after hot isostatic pressing was explored. It is of great significance for subsequent research.

2. Experimental materials and methods

2.1. Material

The material used in the experiment is Ti48Al2Cr2Nb alloy powder provided by Beijing Zhonghang Maite Company. The particle size is 20–60 μm. The composition of Ti48Al2Cr2Nb alloy powder is shown in Table 2. The SLM forming equipment model is EP150, the forming process is scanning speed 900 mm/s and laser power 120 W, and the substrate preheating temperature is 140 °C. After SLM forming, a block with a size of 10 mm × 10 mm × 10 mm was cut off from the substrate by wire cutting as a sample.

Table 2. Chemical composition table of Ti48Al2Cr2Nb alloy powder.

Element	Ti	Al	Cr	Nb
Ti48Al2Cr2Nb (wt %)	bal	32.5–36.7	3.8–5.2	2.3–3.2

2.2. Hot isostatic pressing

The high content of α_2-Ti_3Al phase in the microstructure of Ti48Al2Cr2Nb alloy formed by SLM is the main reason for the brittleness of the alloy after forming. Because the Poisson's ratio of α_2-Ti_3Al phase is larger, the Young's modulus and shear modulus are lower. The hot isostatic pressing treatment is used to reduce the α_2-Ti_3Al phase in the alloy. Before hot isostatic pressing, DSC thermogravimetric analysis is performed to determine the temperature of hot isostatic pressing.

DSC (Differential scanning calorimetry) is a thermal analysis technique used to measure the thermal response of a sample during heating or cooling. It can be used to study the thermal properties of materials, such as melting point, glass transition temperature, crystallization temperature, thermal stability, *etc*. The principle of DSC analysis is to place the sample and the reference in two separate heaters, and measure the thermal response of the sample by comparing the temperature difference between the two heaters. When the sample absorbs or releases heat, it causes temperature differences, which are measured and recorded. By comparing the thermal response of the sample and the reference, the thermal properties of the sample can be determined.

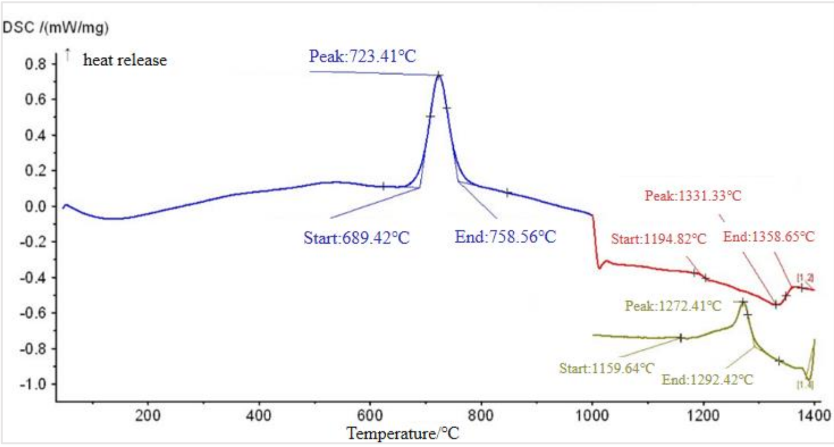

Figure 1. DSC curve of Ti48Al2Cr2Nb alloy formed by SLM.

In this experiment, the phase transition temperature of the alloy was determined by differential scanning calorimetry (DSC). The results are shown in Figure 1. The curve can be divided into three stages. The first stage (0–1000 °C) is the temperature-rising curve, the temperature rise rate is 20 °C/min, and there is an obvious exothermic peak in this stage. It can be seen from the phase diagram and related literature that phase transition occurs at 724.41 °C, and the equilibrium microstructure of the alloy at this temperature is α_2 phase and a small amount of γ phase. Therefore, the phase becomes: $\alpha_2 \rightarrow \gamma$; The second stage (1000–1400 °C) is the temperature-rising curve. When the temperature rises to 1331.33 °C, an endothermic peak appears. The temperature is the temperature at which the α phase begins to transform, the eutectoid temperature Te is 1194.82 °C, and the temperature 1358.85 °C is the temperature at which the alloy enters the α single-phase region. The phase transition occurs here: $\alpha_2+\gamma \rightarrow \alpha$; Stage 3 (1400–1000 °C) is the cooling curve, and the phase transition occurs here corresponds to the phase transition of stage 2, which is eutectoid phase transition: $\alpha \rightarrow \alpha_2+\gamma$. In addition, some phase transitions occur near the eutectoid phase transition in the literature, and this peak is not shown in this DSC test. The reason is that the reaction occurs above 1400 °C in the alloy.

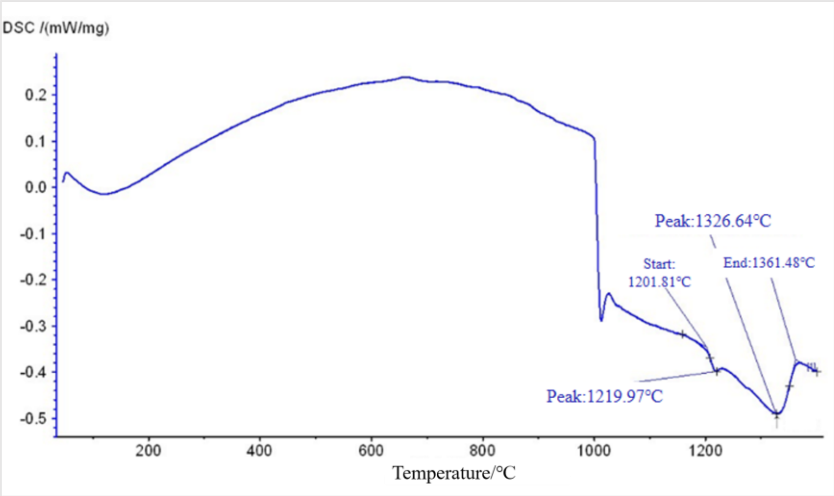

Figure 2. DSC curve of Ti48Al2Cr2Nb alloy formed by SLM after HIP treatment.

The temperature of this hot isostatic pressing treatment is 1225 °C, which is higher than the eutectoid temperature Te (1195 °C) of stage 2 in Figure 2. It can be considered that the near γ treatment is carried out, which is consistent with the conclusion that the content of γ phase accounts for 92.95% after hot isostatic pressing. At the same time, because the phase content after hot isostatic pressing is very small, the phase transition peak appearing in stage one in the previous figure does not appear.

3. Results and discussion

3.1. Friction and wear properties

Wear rate and friction coefficient are important indexes to evaluate the friction properties of materials. Figure 3 is the wear rate of Ti48Al2Cr2Nb alloy and Ti48Al2Cr2Nb alloy after hot isostatic pressing under the load of 20 N and different sliding speeds (200 r/min, 300 r/min and 400 r/min). It can be seen from the figure that under the same 20 N load, the wear rate of Ti48Al2Cr2Nb alloy under SLMed and HIPed treatment decreases with the increase of rotation speed (SLMed represents only selective laser melting, HIPed represents hot isostatic pressing after forming). The increase of rotation speed means the increase of sliding speed, which is consistent with the study of YANG [19]. The wear rate of the sample after hot isostatic pressing is significantly lower than that of the sample without hot isostatic pressing. The reason for this trend is that the friction heat is generated during the friction process, and the friction work during the sliding process generates heat. The expression is as follows:

$$q = \mu F v \quad (1)$$

Here, q represents the total energy (J/s) generated during the friction process, F represents the additional load (N) added during the friction process, and v represents the sliding speed.

The friction heat generated during the wear process will increase the temperature of the sliding interface. The maximum temperature generated has the following relationship with the sliding speed and additional load [20]:

$$T_{max} = T_0 + aF^{\frac{1}{4}}v^{\frac{1}{2}} \tag{2}$$

Where T_{max} is the maximum temperature of the friction interface, F is the load (N) added to the friction process, v is the sliding speed (m/s), T_0 and a depend on $F^{\frac{1}{4}}v^{\frac{1}{2}}$ the size, $F^{\frac{1}{4}}v^{\frac{1}{2}} > 2.8$, $T_0 = -191$ K, a = 210.5 ; $F^{\frac{1}{4}}v^{\frac{1}{2}} < 2.8$, $T_0 = 290$ K, a = 15.1.

It can be obtained from Equation (2) that the temperature of the wear surface during friction is positively correlated with the sliding speed, which will increase with the increase of the sliding speed. The friction heat generated during the sliding process will increase the temperature of the sliding contact surface. As the temperature continues to increase, a hardened layer or an oxide layer will be formed on the worn surface, which will effectively reduce the contact area between the friction stainless steel ball and the Ti48Al2Cr2Nb alloy, resulting in a decrease in the wear rate.

Mechanically mixed layer (MML) refers to a layer with high strength and hardness formed on the surface of the alloy, which is usually prepared by mechanical processing or friction stirring. MML is usually composed of metal particles on the surface of Ti-Al alloy and oxide particles attached to it. These particles are strongly plastically deformed and mixed during machining or friction stirring to form a uniform, dense, high-strength and high-hardness layer. The thickness of MML is usually between a few microns and tens of microns, which can significantly improve the surface hardness, wear resistance and corrosion resistance of Ti-Al alloy, thereby improving its service life and performance.

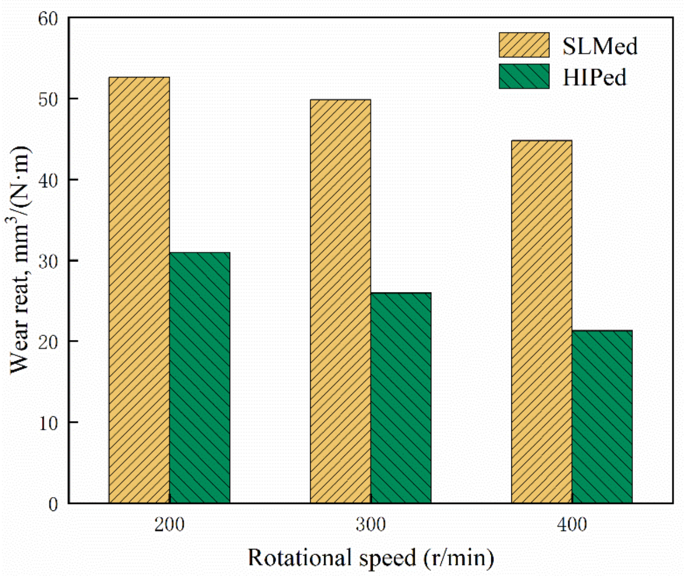

Figure 3. Wear rate of Ti48Al2Cr2Nb alloy treated with SLMed and HIPed at different rotational speeds.

Figure 4 and Figure 5 are the friction coefficients of the samples in SLMed and HIPed states, respectively. The results show that under the same treatment conditions, the friction coefficient of the samples under the two treatment conditions generally decreases with the increase of the rotational speeds. At the rotational speeds of 200 r/min and 300 r/min, the friction coefficient of the SLMed sample is not much different, about 0.9; the friction coefficient decreased significantly to 0.4 at 400 r/min. In the HIPed sample, the friction coefficient is 0.8 when the rotational speeds is 200 r/min, and the friction coefficient is significantly reduced when the rotational speeds is 300 r/min and 400 r/min, but the difference between the two is not large, close to 0.6.

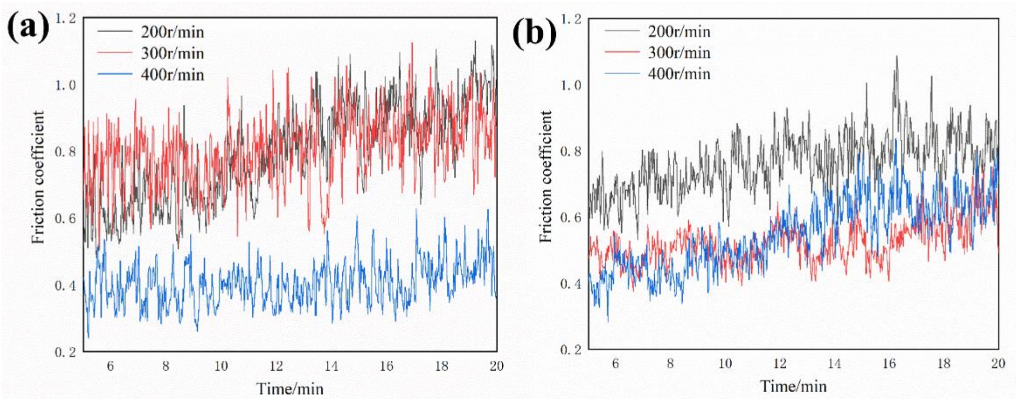

Figure 4. Friction coefficient of SLM sample at different rotation speeds: (a) SLM samples; (b) HIP sample.

3.2. Friction and wear structure

Figure 5 is the SEM morphology and outline drawing of the worn surface of the SLM sample under 20 N load and 200, 300, 400 r/min rotational speeds. As shown in Figure 5(a), The wear surface is smooth, with a large number of deep grooves parallel to the sliding direction and a small amount of oxide fragments, and there is a large degree of material removal, outline drawing. Figure 5(b) is a two-dimensional outline drawing of 5(a), and the maximum depth of wear reaches 50.7 μm. As the rotational speeds increases, the sliding speed increases, the groove gradually narrows, and wrinkle-like structures begin to appear. This is due to plastic deformation and more wear debris, and the maximum depth of wear reaches 57.6 μm, as shown in Figure 5(c) and (d).

When the rotational speeds is 400 r/min, a large number of wrinkle-like structures appear in the SEM morphology of the wear surface. At this time, it can be seen from Figure 4 that the friction coefficient decreases significantly. This is due to the appearance of these structures, which effectively reduces the effective metal contact area between the friction ball and the surface of the wear material. Although the maximum depth of the wear surface also increases with the increase of rotational speeds and sliding speed, it can be seen from Figure 3 that the wear rate gradually decreases, which is due to the increase of the denominator sliding speed in the wear rate formula and the appearance of the mechanical mixing layer.

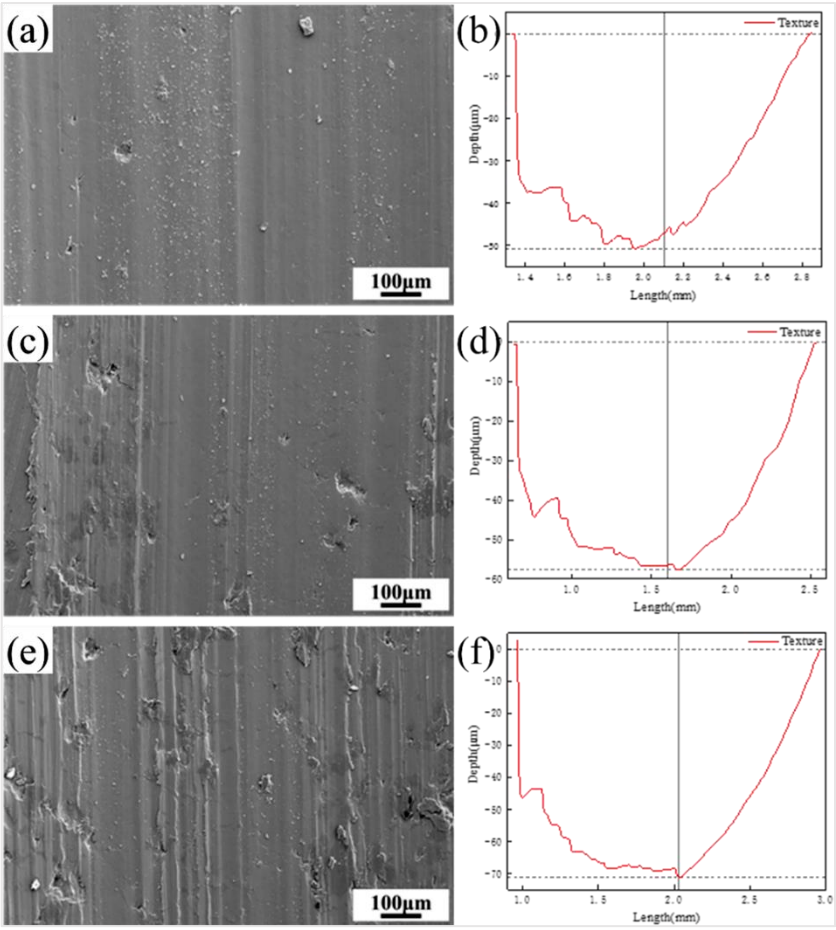

Figure 5. Wear surface morphology and profile of SLM samples at different rotation speeds: (a), (b) 200 r/min; (c), (d) 300 r/min; (e), (f) 400 r/min.

Figure 6 is the SEM morphology and outline drawing of the worn surface of the HIPed sample under 20 N load and 200, 300, 400 r/min rotational speeds. As shown in Figure 6(a), the wear surface is relatively smooth, with a large number of deep grooves and a small amount of oxidation debris, and the grooves are not well matched with the sliding direction. The groove has a large degree of material removal, which is the combination of abrasive wear and oxidation friction and wear. Figure 6(b) is a two-dimensional outline drawing of Figure 6(a), and the maximum depth of wear reaches 42.5 μm. As the rotational speeds increases, the sliding speed increases, the groove gradually narrows, and a mechanical mixing layer begins to appear. This is due to plastic deformation and more wear debris. The maximum depth of wear reaches 44.6 μm, as shown in Figure 6(c) and Figure 6(d).

When the rotational speeds is 400 r/min, the mechanical mixing layer and large flake debris appear in the SEM morphology of the wear surface. At this time, it can be seen from Figure 4 that the friction coefficient decreases significantly. This is due to the appearance of these structures, which effectively reduces the effective metal contact area between the friction ball and the surface of the wear material. Although the maximum depth of the wear surface also increases with the increase of rotational speeds and sliding speed, it can be seen from Figure 3 that the wear rate gradually decreases, which is due to the increase of the denominator sliding speed in the wear rate formula and the appearance of the mechanical mixing layer.

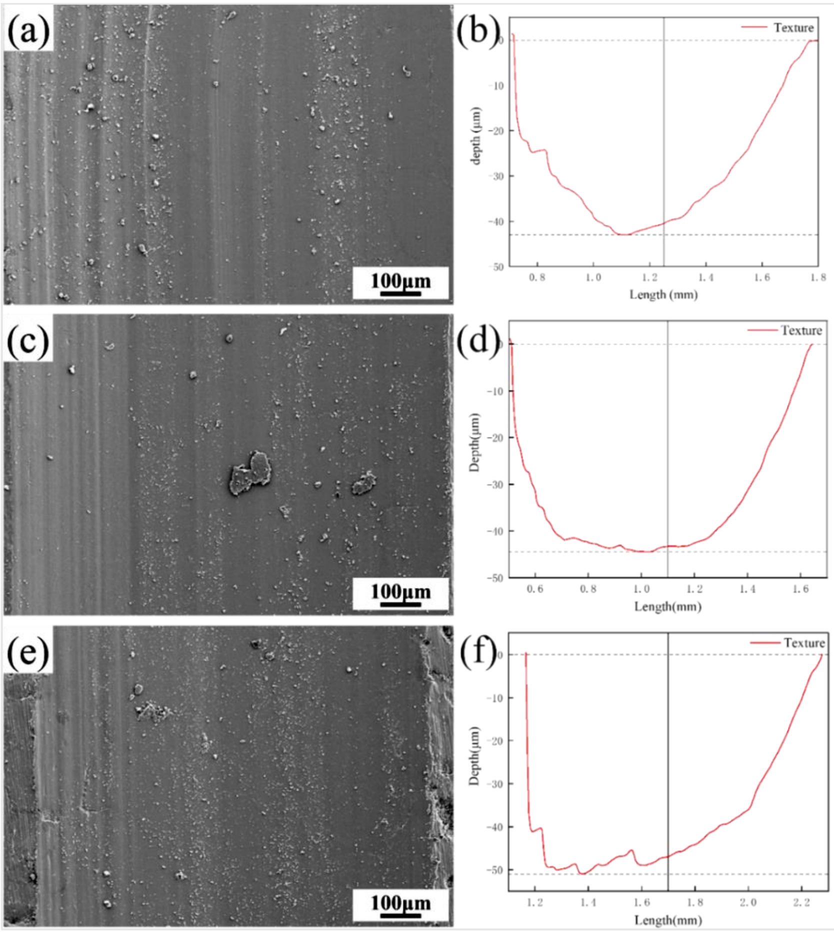

Figure 6. Wear surface morphology and profile of HIP samples at different rotation speeds: (a), (b) 200 r/min; (c), (d) 300 r/min; (e), (f) 400 r/min.

Figure 7(a) and (b) are the micro-morphology of the corresponding SEM wear debris after different treatments at a speed of 400 r/min. Facts show that the number and size of wear debris in SLMed samples are larger than those in HIPed samples. The point scanning results of point A and point B of the SLMed sample show that the oxygen content of the large particle wear debris is much higher than that of the small particle wear debris, that is, the small particle wear debris is mainly abrasive wear, and the large particle wear debris is mainly oxidative wear. Some large flake wear debris appeared in the HIPed sample, and the oxygen content was higher than that of the SLMed sample, indicating that the oxidation wear was serious. Moreover, the flake wear debris reduces the effective metal contact area on the surface of the worn material, so the wear rate and friction coefficient are low.

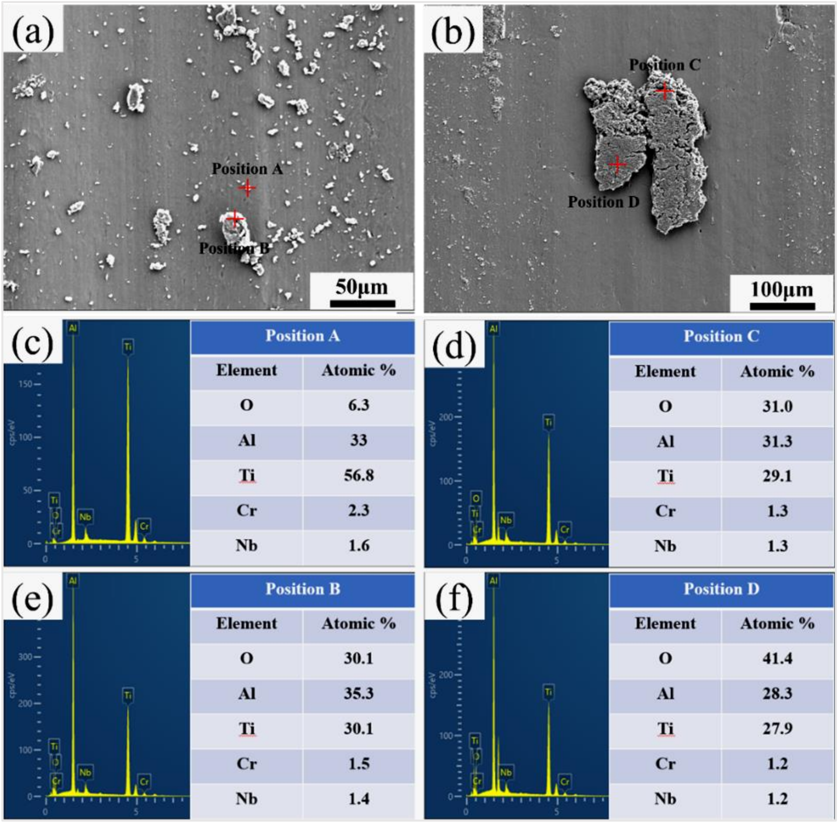

Figure 7. SEM Abrasion Chip Morphology Map Corresponding to Rotating Speed of 300 r/min: (a) HIPed Sample; (b) SLM Sample; (c) EDS Oxygen Content Analysis at Point A; (d) EDS Oxygen Content Analysis at Point B; (e) EDS Oxygen Content Analysis at Point C; (f) EDS Oxygen Content Analysis at Point D.

4. Conclusions

In this paper, the effects of different rotational speeds on the friction and wear properties of SLM formed Ti48Al2Cr2Nb alloy under the same load and the effect of HIP treatment on the friction and wear properties of Ti48Al2Cr2Nb alloy were discussed. The wear mechanism of Ti48Al2Cr2Nb alloy under different conditions was explored.

With the increase of rotational speeds, the wear rate of SLM formed Ti48Al2Cr2Nb alloy decreases and the friction coefficient decreases gradually. This is due to the formation of a mechanical mixing layer, which reduces the contact area between the friction material and the wear surface and improves the tribological properties.

The wear rate of the alloy after HIP treatment is greatly reduced, and some large flake wear debris appear on the wear surface. This is because the hardness of the material after HIP treatment becomes larger, and it has strong wear resistance and cutting resistance. However, the internal crystal structure is relatively dense and orderly, which is difficult to plastically deform and prone to brittle fracture.

At the rotational speeds of 400 r/min, the friction coefficient of Ti48Al2Cr2Nb alloy without HIP treatment reached the lowest value of 0.4. The reason is that the sample has low hardness and good plasticity. At high rotation speed, the material will deform, plastic flow and disperse mixing, forming a large number of thick mechanical mixing layers.

Acknowledgment

This work is financially supported by the National Natural Science Foundation of China (No. U22A20192), the Natural Science Foundation of Shanxi Province (20210302123064), and the special fund for Science and Technology Innovation Teams of Shanxi Province.

Conflicts of interests

The authors declare that they have no known competing financial interests or personal relationships that could have appeared to influence the work reported in this paper.

Authors' contribution

Conceptualization, Zhanyong Zhao; methodology, Zhanyong Zhao, Wenbo Du and Yongli Guo; software, Yongli Guo; validation, Peikang Bai; formal analysis, Zhen Zhang and Liqing Wang; investigation, Wenbo Du; resources, Zhanyong Zhao and Peikang Bai; data curation, Kai Ma; writing—original draft preparation, Zhanyong Zhao; writing— review and editing, Wenbo Du and Yaohao Du; visualization, Liqing Wang and Zhen Zhang; supervision, Peikang Bai; project administration, Peikang Bai; funding acquisition, Peikang Bai. All authors have read and agreed to the published version of the manuscript.

Data availability

The data supporting the findings of this study are available from the corresponding author on request.

References

[1] Liu P, Xie J, Wang A. Recent research progress in TiAl matrix composites: a review. *J. Mater. Sci.* 2022, 57(34):16147–16174.
[2] Xu R, Li M, Zhao Y. A review of microstructure control and mechanical performance optimization of γ-TiAl alloys. *J. Alloys Compd.* 2023, 932:167611.
[3] Li Y, Yang C, Zhao H, Qu S, Li X, *et al.* New developments of Ti-based alloys for biomedical applications. *Materials* 2014, 7(3):1709–1800.
[4] Thellaputta GR, Chandra PS, Rao CSP. Machinability of nickel based superalloys: a review. *Mater. Today Proc.* 2017, 4(2):3712–3721.
[5] Sourani F, Enayati MH, Taghipour M. High-temperature oxidation and wear behavior of (Fe,Cr) Al intermetallic compound and (Fe,Cr) Al-Al2O3 nanocomposites. *J. Mater. Eng. Perform.* 2021, 30:3654–3669.
[6] Nie XY, Zhao KN, Li HX, Du Q, Zhang JS, *et al.* Comparisons of interface microstructure and mechanical behavior between Ti/Al and Ti-6Al-4V/Al bimetallic composite. *China Foundry* 2015, 12(1):1–8.
[7] Huang LJ, Geng L, Peng HX. Microstructurally inhomogeneous composites: Is a homogeneous reinforcement distribution optimal?. *Prog. Mater. Sci.* 2015, 71:93–168.
[8] Su YQ, Liu T, Li XZ, Chen R, Guo J, *et al.* The evolution of seeding technique for the

lamellar orientation controlling of γ-TiAl based alloys. *Acta Metall. Sin.* 2018, 54(5):647–656.

[9] Genc O, Unal R. Development of gamma titanium aluminide (γ-TiAl) alloys: A review. *J. Alloys Compd.* 2022, 929:167262.

[10] Schütze M. Single-crystal performance boost. *Nat. Mater.* 2016, 15(8):823–824.

[11] Zhao P, Li X, Tang H, Ma Y, Chen B, *et al.* Improved high-temperature oxidation properties for Mn-containing beta-gamma TiAl with W addition. *Oxid. Met.* 2020, 93:433–448.

[12] Pan Y, Lu X, Hui T, Liu C, Liu B, *et al.* High-temperature oxidation behaviour of TiAl alloys with Co addition. *J. Mater. Sci*. 2021, 56:815–827.

[13] Shu S, Qiu F, Tong C, Shan X, Jiang Q. Effects of Fe, Co and Ni elements on the ductility of TiAl alloy. *J. Alloys Compd.* 2014, 617:302–305.

[14] Bauer J, Rogl P, Perrin A, Bohn M, Wolf W, *et al.* TiAl-based alloys with nickel. *Intermetallics* 1996, 4(1):71–76.

[15] Yoshihara M, Kim YW. Oxidation behavior of gamma alloys designed for high temperature applications. *Intermetallics* 2005, 13(9):952–958.

[16] Bartolotta P, Barrett J, Kelly T, Smashey R. The use of cast Ti−48Al−2Cr−2Nb in jet engines. *Jom* 1997, 49(5):48–50.

[17] Singh V, Mondal C, Sarkar R, Bhattacharjee PP, Ghosal P. Effects of Cr alloying on the evolution of solidification microstructure and phase transformations of high-Nb containing γ-TiAl based alloys. *Intermetallics* 2021, 131:107117.

[18] Imayev RM, Imayev VM, Oehring M, Appel F. Alloy design concepts for refined gamma titanium aluminide based alloys. *Intermetallics* 2007, 15(4):451–460.

[19] Yang K, Shi X, Huang Y, Wang Z, Wang Y, *et al.* The research on the sliding friction and wear behaviors of TiAl-10 wt % Ag at elevated temperatures. *Mater. Chem. Phys.* 2017, 186:317–326.

[20] An J, Sun W, Niu XD. Dry sliding wear behavior and a proposed criterion for mild to severe wear transition of Mg–3Al–0.4Si–0.1Zn alloy. *Tribol. Lett.* 2017, 65:98.